

# Numerical calculation of the vortex–columnar-defect interaction and critical currents in extreme type-II superconductors—a two-dimensional model based on the Ginzburg–Landau approximation

S M Maurer, N-C Yeh and T A Tombrello

Department of Physics, California Institute of Technology, Pasadena, CA 91125, USA

Received 16 April 1998, in final form 3 June 1998

**Abstract.** We extend our previous one-dimensional Ginzburg–Landau calculations of the pinning energy of vortices to two dimensions, in order to achieve an understanding of the pinning forces exerted on vortices by defects. By minimizing the free energy using a relaxation scheme, we obtain the spatial variation of the order parameter and supercurrents for a vortex in the vicinity of a cylindrical defect in an extreme type-II superconductor. The resulting two-dimensional field distributions provide a direct mapping of the spatial dependence of the vortex–defect pinning potential, thereby yielding the pinning force and depinning current as a function of the defect size and magnetic field. We also use periodic boundary conditions in the two-dimensional Ginzburg–Landau equations to solve for the known vortex–vortex interaction, in order to verify the resolution and accuracy of our approach for extreme type-II superconductors. Our direct numerical derivation of the pinning force per vortex is shown to be applicable to a wide range of magnetic fields and columnar-defect densities, and the calculated results are consistent with experimental observation.

## 1. Introduction

Columnar defects with radii comparable to the superconducting coherence length have been shown to be efficient pinning sites for vortices in type-II superconductors [1–4]. The effects of columnar defects on the enhancement of the critical current density  $J_c$  [5, 6], and the increase of the vortex phase transition temperature [7] and the onset temperature ( $T_{irr}$ ) for vortex pinning, are of both fundamental interest and practical importance. It has been observed recently that in both  $\text{YBa}_2\text{Cu}_3\text{O}_7$  and  $\text{Bi}_2\text{Sr}_2\text{CaCu}_2\text{O}_8$  single crystals, there is a maximum density of heavy-ion-irradiated columnar defects above which no further increase of  $J_c$  or  $T_{irr}$  can take place [8]. Although there are phenomenological descriptions for the interaction between vortices and the columnar defects which are extended static disorder, and an upper bound for the benefit of introducing columnar defects is believed to exist [8], direct theoretical verification of these issues is still lacking. This situation is in contrast to the establishment of microscopic vortex–pin interaction based on the Gorkov theory [9, 10] for the presence of random point disorder.

We have recently performed calculations for the interaction between vortices and columnar defects by solving the one-dimensional Ginzburg–Landau equations in a cylindrically symmetric system [11], and have derived the pinning potential and depinning temperature as functions of the defect size and defect conductivity. In this work we extend

our previous one-dimensional model to two dimensions, in order to map out the spatial variation of the pinning potential and to obtain the corresponding pinning force per unit length ( $f_{pin}$ ) and the depinning critical current density ( $J_c$ ). Our numerical integration using a relaxation scheme [12] yields a detailed description of the behaviour of the order parameter and supercurrents near a columnar defect, and thus a fundamental scheme for calculating the spatial variation of the vortex–defect pinning potential. In contrast to phenomenological analyses of the vortex–pin interaction [6] which are only concerned with the changes in the potential energy due to the presence of columnar defects, our calculations go beyond the geometric considerations by explicitly including both the kinetic and potential energies of the vortex–pin system. In addition, our two-dimensional calculations allow a quantitative study of the interplay between vortex–vortex interactions and vortex–defect interactions on the microscopic scale, which has not been addressed in most numerical simulations carried out by other research groups [12–16]. More specifically, the effect of defects on the pinning of vortices is often described in terms of a ‘disorder parameter’  $\gamma$ , defined as [6]

$$\gamma \equiv f_{pin}^2 n_i \xi^2 \quad (1)$$

where  $n_i$  is the volume density of pinning defects. Various important physical properties associated with the vortex–pin interaction, such as the critical current density, depinning temperature, and vortex correlation lengths, can be determined if  $\gamma$  is known [6]. In contrast to most numerical calculations which *assume* the pinning force  $f_{pin}$  and the disorder parameter  $\gamma$ , our approach directly *calculates* the quantity  $f_{pin}$  by using the two-dimensional Ginzburg–Landau equations and proper boundary conditions.

This paper is structured as follows. Section 2 describes the numerical method used to set up and compute the physical problems of the two-dimensional vortex–pin interaction; section 3 presents the results of the calculations, discusses the applicability and limitations of the model, and compares our results with those obtained by other research groups and with experiments; and section 4 summarizes the key findings and some feasible extension of this work.

## 2. Methods and justifications

We shall limit ourselves to studies of extreme type-II superconductors such as the high-temperature superconductors whose Ginzburg–Landau parameter  $\kappa$  is very large. We shall also limit ourselves to large applied fields  $H_a$ , so that the magnetization of the superconductor is nearly zero. Hence, it is a good approximation to assume that the magnetic induction  $B$  is constant everywhere in the superconductor. Under such approximations, the relevant free-energy density ( $\mathcal{F}$ ), expressed in terms of the superconducting order parameter  $\Psi$  and the vector potential  $\mathbf{A}$ , becomes

$$\mathcal{F} = \frac{H_c^2}{8\pi} \left( \frac{|\Psi|^4}{|\Psi_\infty|^4} - 2 \frac{|\Psi|^2}{|\Psi_\infty|^2} + 2\xi^2 \left| \left( \frac{\nabla}{i} - \frac{e^*}{\hbar c} \mathbf{A} \right) \frac{\Psi}{|\Psi_\infty|} \right|^2 \right) \quad (2)$$

where  $\Psi_\infty$  is the order parameter in an infinite sample,  $H_c$  is the thermodynamic critical field, and  $\xi$  is the superconducting coherence length.

Rather than using this expression to derive the Ginzburg–Landau equations via the variational principle, we will minimize the free energy directly, by relaxing the energy iteratively to its minimum value. To do this, we will evaluate the free energy on a uniform grid, with a spacing between points given by  $\xi/n_\xi$ , where  $n_\xi$  is the number of grid points in one coherence length. The length scale used in this paper will be given in units of the

quantity

$$d \equiv 2\sqrt{\Phi_0/(\pi H_a)}$$

which is the distance between neighbouring circular cells, defined in reference [11] and to be described in more detail below, and is approximately equal to the Abrikosov vortex lattice constant. Here  $\Phi_0$  is the flux quantum, and  $H_a$  is the applied magnetic field. We will also use the reduced units in which magnetic fields are measured in units of  $\sqrt{2}H_c$ , and  $f \equiv \Psi/|\Psi_\infty|$ . Thus, the free energy may be rewritten as follows:

$$\mathcal{F} = \frac{1}{16\pi} (|f|^4 - 2|f|^2 + 2n_\xi^2 |(\mathbf{i}\nabla + \mathcal{A})f|^2). \quad (3)$$

Note that in terms of the vector potential used in equation (2), the new vector potential in equation (3) is  $\mathcal{A} = [2\pi\xi/(n_\xi\Phi_0)]\mathbf{A}$ . Equation (3) is now easily discretized in a gauge-invariant form and then minimized, lattice point by lattice point. We do so iteratively to solve for the spatial variation of the complex order parameter.

As in reference [11], we will at first limit ourselves to circular cells. The range of validity of this approximation has been discussed previously [11], and may be briefly summarized as follows. First, both the defect size  $a$  and the superconducting coherence length  $\xi$  must be much smaller than the vortex–vortex separation  $d$  ( $a, \xi \ll d$ ). Second, the defect distribution has to be either regular or commensurate with the vortex lattice, or completely random and satisfying one of the conditions  $H_a \ll B_\phi$  and  $H_a \gg B_\phi$ , where  $B_\phi \equiv \Phi_0 n_\phi$  is the matching field, with  $n_\phi$  being the areal density of columnar defects. In most of the following calculations of the vortex–defect interaction, we shall focus on the two-dimensional solutions in the circular-cell approximation. In section 3.5, an alternative approach using periodic boundary conditions will be employed for the two-dimensional vortex lattice in the absence of defects.

We solve the two-dimensional circular-cell problem by considering the following boundary conditions: first, the magnitude of the order parameter is assumed to be the same around the outer periphery of a cell, and is so chosen that the total energy is minimized. (Usually, it will be accurate enough to simply take  $f = 1$ .) The phase around the outer periphery is assumed to vary continuously from 0 to  $2n\pi$ , where  $n$  is the number of vortices inside the circular cell. Thus, the outer boundary conditions ensure no preferable direction from the origin. We also note that under the given boundary conditions, the vortices exterior to the boundary (outside the region of integration) are always effectively pinned. Such constraints are an adequate approximation of the vortex system if  $H_a \leq B_\phi$ , i.e. as long as there are enough pinning sites for all of the vortices. In the limit  $H_a \gg B_\phi$ , on the other hand, our numerical solutions to the single-vortex and single-pin scheme are only applicable if we consider the following correction to the pinning force: at low temperatures and for  $H_a \gg B_\phi$ , columnar defects yield effectively two-dimensional collective pinning effects on vortices [6], and the critical current density ( $J_c^{2D}$ ) in the two-dimensional collective pinning regime is approximately given by  $J_c^{2D} \approx j_{pc}(d/R_c)$  [6], where  $j_{pc}$  is the planar critical current density, and  $R_c$  is the two-dimensional collective pinning length [6]. Hence, it can be shown that

$$\frac{J_c^{2D}}{J_0} \approx \frac{4\gamma d^2}{\varepsilon_0^2 d_c} \propto \left(\frac{n_\phi}{H_a}\right) f_{pin}^2 \quad (4)$$

where  $J_0 \equiv cH_c/(3\sqrt{6}\pi\lambda)$  is the depairing current density [6],  $\varepsilon_0 \equiv \Phi_0^2/(4\pi\lambda)^2$ , and  $d_c$  is the  $c$ -axis lattice constant of the cuprate superconductor. Equation (4) predicts a critical current density that increases with the increasing areal defect density  $n_\phi$ , and decreases with the increasing applied magnetic field  $H_a$  [6], consistently with the experimental finding for

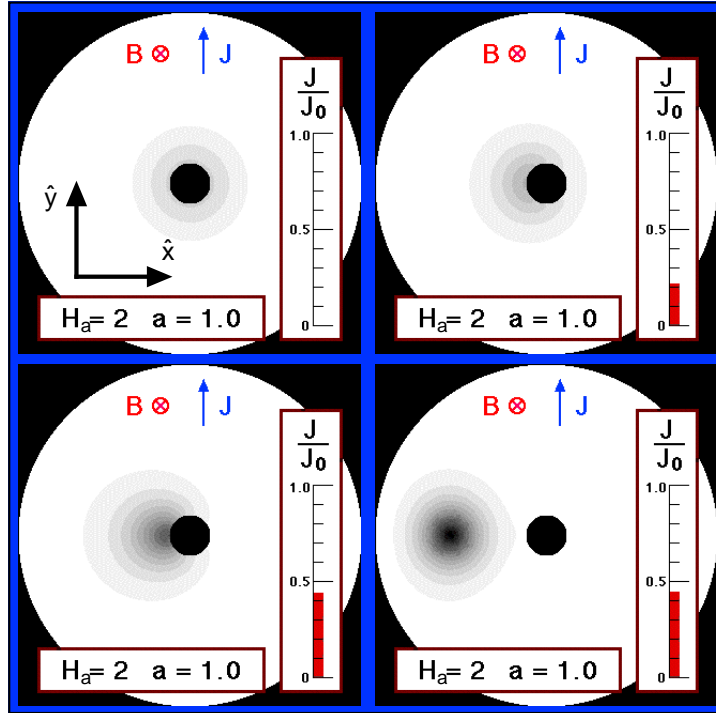


**Figure 1.** The spatial variation of the order parameter as a function of the current, for  $H_a = 2\sqrt{2}H_c$  and  $a = \xi$ . The four frames correspond to  $J = 0$ ,  $J = 0.22J_0$ , and  $J = 0.44J_0$  just before and after depinning occurs. The white area corresponds to an amplitude of the order parameter  $f$  near 1. The darker the shading, the closer the amplitude is to 0.

$H_a \gg B_\phi$ . In the following calculations, we shall concern ourselves with the numerical solutions to the problem of one defect and one vortex per cell. We have discussed how the calculated results for  $f_{pin}$  may be applied to the vortex–pin interaction over a wide range of magnetic fields.

As stated previously, the area  $S$  of each cell is determined by the applied magnetic field  $H_a$ , such that  $S = n\Phi_0/H_a$ . To investigate the effect of an external transport current on the pinned vortices (at least for sufficiently small currents), we assume that both the applied field and columnar defects are aligned along the  $z$ -axis, and a uniform current is imposed crossing the cell and moving vertically along the  $\hat{y}$ -axis (see figure 1). This requirement can be achieved by adding a term to the phase of the order parameter on the outer boundary, given by

$$\Delta\phi = -\frac{Jy}{(3/2)\sqrt{3}|f|^2} \quad (5)$$

where  $J$  is a current density measured in units of the depairing current density  $J_0$  [6].

Finally, we can treat any number of defects on the inside of the integration region using boundary conditions given by de Gennes for a bulk-superconductor–bulk-normal-metal interface [17]:

$$\left(\frac{\hbar}{i}\nabla - \frac{e^*}{c}\mathbf{A}\right)\Psi|_n = \frac{i\hbar}{b}\Psi. \quad (6)$$

Here  $1/b$  is a real proportionality constant and has the dimensions of inverse distance. As shown by de Gennes [17], for a superconductor/insulator (or vacuum) interface, the parameter  $1/b$  can be taken as zero, implying no current flowing normal to the boundary between a columnar defect and the surrounding superconducting material. We shall take this limit because the columnar defects induced by high-energy heavy ions are known to be insulating [1]. In addition, we will also limit ourselves to the large- $\kappa$ , high- $H_a$  case in which the magnetization is zero and  $B = H_a = \text{constant}$  everywhere.

### 3. Results and discussion

#### 3.1. The pinning force derived from an applied current

We consider a defect at the centre of the circular region, and let the outer boundary dictate the position of one vortex. This condition effectively simulates the situation of  $H_a = B_\phi$  for a regular distribution of columnar defects. As stated in the previous section, the effective pinning force per vortex per length derived for this special case may be generalized to the situation of randomly distributed columnar defects with either  $H_a < B_\phi$  or  $H_a \gg B_\phi$ .

The minimum-energy requirement in the absence of an applied current will place the vortex at the centre, where the defect is. If a net current crossing the cell is added to the system, as described according to the outer boundary condition given by equation (5), we may study the evolution of the solution as the current is slowly increased. The spatial variation of the order parameter as a function of current is shown in figure 1, while the position of the vortex, measured radially from the centre of the cell and defined as the place where the order parameter is zero, as a function of the applied current and for different defect sizes, is plotted in figure 2.

We note that in the absence of pinning defects, vortices will be displaced linearly with the applied currents, at least for sufficiently small vortex displacements from the centre of the cell, as illustrated in figure 2. For large applied currents, on the other hand, vortex displacement no longer increases linearly with the applied current  $J$ . This deviation from linearity in the large-current limit (see figure 2) is the result of two contributing factors. One is due to the assumption of pinned vortices exterior to the circular cell, which gives rise to a net force on the vortex within the cell if the vortex is displaced away from the centre. The other is the constant phase on the outer boundary, which prevents the inner vortex from leaving the cell under any applied currents. In other words, in the absence of any defects in the circular cell, we are solving for a static solution in which two forces on the inner vortex balance each other: the Lorentz force due to the applied current, and the net pinning force exerted by the external vortices when a Lorentz force is applied to both the interior vortex and the effectively pinned exterior vortices.

In the presence of a columnar defect, an additional attractive pinning force due to the vortex–pin interaction must be considered, and figures 1 and 2 show that the vortex remains pinned by the defect up to a critical current  $J_c$ . Once this critical current is reached, the vortex is suddenly depinned and jumps towards the cell boundary where the presence of the surrounding stationary vortices prevents it from moving out further. Once the vortex is depinned, we find that the existence of the defect inside the cell is no longer relevant. In other words, for sufficiently strong currents, the position of the vortex only depends on the configuration of the surrounding vortices, independently of the existence of the defect inside the cell, as manifested by the merging curves in figure 2 for different defect radii in the large-current limit. We also note that the critical current density  $J_c$  increases with increasing defect radius  $a$ , provided that the defect size is comparable to the coherence

length. This finding is consistent with our previous one-dimensional numerical calculations [11]. However, our calculations suggest that the increase in  $J_c$  with the defect radius  $a$  is substantially smaller than the phenomenological estimate in reference [6] which asserts that  $J_c \propto a^2$ . This discrepancy may be attributed to an overestimate of the pinning energy in the latter, where the simple geometric consideration of the potential energy [6] does not take into consideration the increasing kinetic energy associated with the larger supercurrents required to screen the increasing magnetic flux in a larger columnar defect. The increasing kinetic energy reduces the effective pinning potential energy gained by enlarging the defect radius.

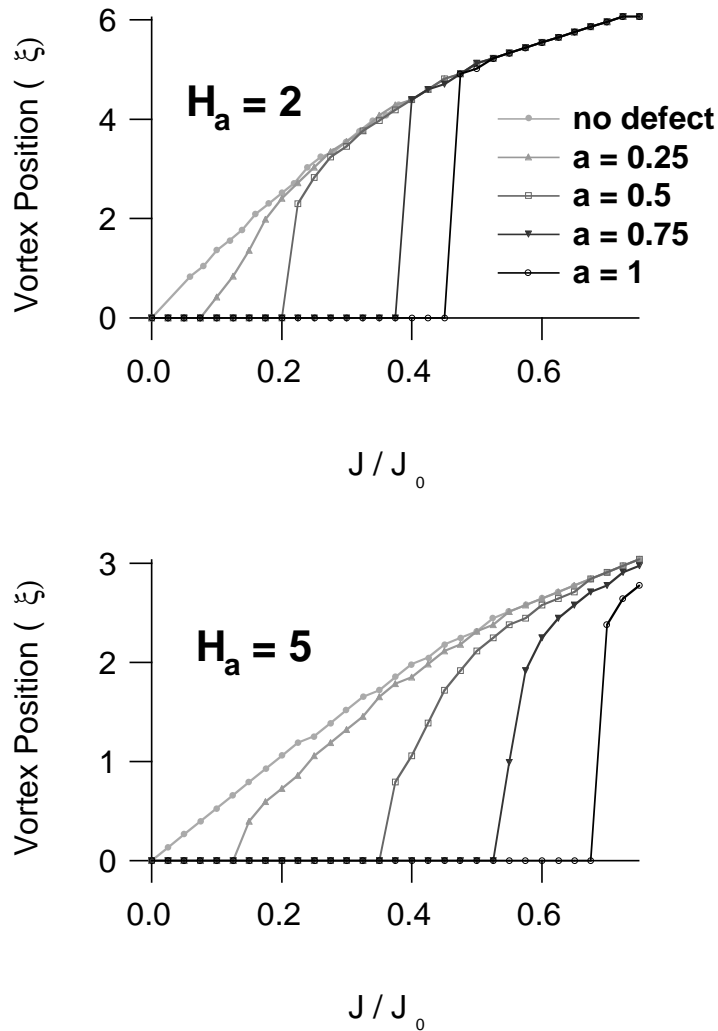


**Figure 2.** The vortex position relative to the centre of the cell as a function of the applied current, for  $H_a = 2\sqrt{2}H_c$ . The curves correspond to no pinning defect, a defect with  $a = 0.5\xi$ , and a defect with  $a = \xi$ . The centre of the vortex remains inside the defect until the current is strong enough to completely depin the vortex. The depinning current for  $a = 0.5\xi$  is consistent with experimental estimates [2].

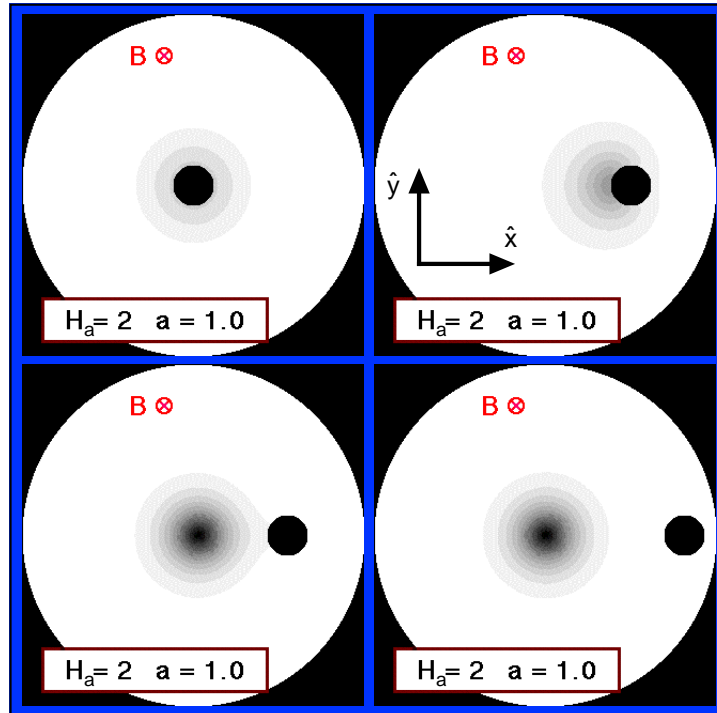


**Figure 3.** The spatial variation of the order parameter as a function of the defect displacement, for  $H_a = 2\sqrt{2}H_c$  and  $a = \xi$ . The four frames correspond to no displacement, displacements of 4.5 and 4.6 coherence lengths (just before and after depinning occurs), and a displacement of almost 7 coherence lengths, respectively. As in figure 1, the shading is lighter for amplitudes nearer zero.

### 3.2. The spatial variation of the vortex–defect pinning potential well

An alternative ‘numerical experiment’ is to depin the vortex by ‘displacing’ the defect, rather than by forcing the pinned vortex with an applied current. With increasing displacement of the defect, the outer boundary, representing the presence of nearby and strongly pinned vortices, competes with the pinning strength of the inner columnar defect, and eventually ‘depins’ the vortex from the columnar defect as the latter moves too close to the boundary. Once depinned, the inner vortex will be kept centred due to the energy considerations. A sample solution with  $H_a = 2$  and  $a = 1.0$  is shown in figure 3, and the corresponding energy densities for various configurations of the defect displacement are shown in figure 4. We note that there is an energy cost involved in displacing the defect away from the centre. As illustrated in figure 4, a rapid increase in energy accompanies the defect displacement, and this is followed by a much more gradual increase in energy after the vortex becomes depinned from the defect. The depth of the energy difference yields an effective pinning potential. This effective pinning potential contains predominantly the effect of the vortex–defect interaction, as well as the net interactions of the surrounding vortices, represented by the outer boundary, with the inner vortex. We note that the latter contributions are much smaller than the former, as manifested by the much smaller increase in energy after the inner vortex is depinned (see figure 4). As a result, we obtain a more accurate estimate of

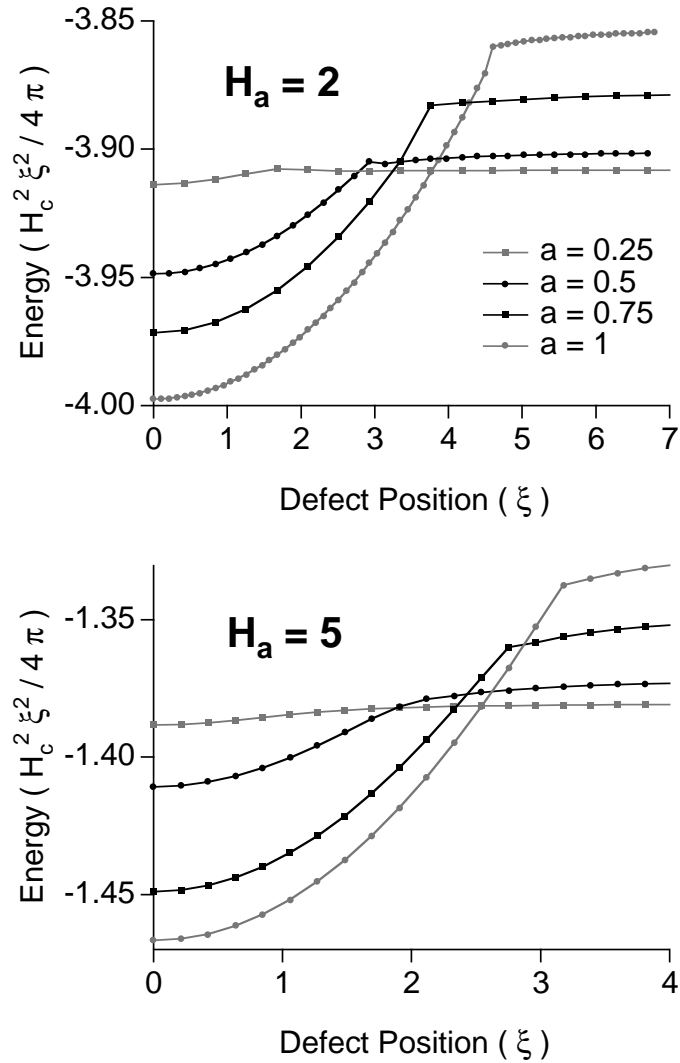


**Figure 4.** The energy per vortex line as a function of the defect displacement, for  $H_a = 2\sqrt{2}H_c$  and  $a = \xi$ .

the depinning force by taking the slope of the effective potential energy—the contribution due to the surrounding vortices will be smaller than for the values obtained from figure 2. We also find that the depth of the pinning potential is the same as that calculated previously using our one-dimensional model [11].

### 3.3. Estimation of the depinning current

As discussed earlier, the critical currents  $J_c$  obtained from figure 2 may be used to estimate the pinning force from a defect, although corrections are obviously needed: the  $J_c$ -values are overestimated since the outer boundary conditions artificially increase the total pinning strength. Indeed, in our solutions, the Lorentz force exerted by the applied current is

balanced both by the pinning force due to the defect and by the repulsion from the surrounding vortices. As stated earlier in this article, better estimates of  $J_c$  may be obtained if we calculate the derivative of the energy relative to the defect displacement in figure 4, because the approach given in figure 4 compares the energy difference among various vortex–pin configurations, which effectively cancels the excess force from the assumption of completely pinned vortices exterior to the cell under consideration. A third possibility for estimating  $J_c$  is to simply record the defect position for which depinning occurs, and then determine what current is necessary to bring a free vortex to that position, using the dependence of the vortex displacement on the applied current given by the ‘no-defect’ curve in figure 2. The corresponding Lorentz force due to that current will be taken as equivalent to the pinning force. However, the pinning force thus derived arises from both the outer boundary and the defect, similarly to in the first method described earlier. Hence, we expect the pinning force to be overestimated using the third method.

For comparison, the pinning force per unit length  $f_{pin}$  from the scheme illustrated in figure 2 is explicitly given by

$$\frac{f_{pin}}{H_c^2 \xi} = \frac{J}{J_0} \frac{2}{3\sqrt{3}}. \tag{7}$$

Similarly, from the maximum slope  $s$  of the potential energy curve in figure 4, we have (where  $s$  is expressed in our dimensionless units)

$$\frac{f_{pin}}{H_c^2 \xi} = 2s. \tag{8}$$

**Table 1.** The depinning force, calculated from the depinning current obtained from figure 2, and calculated from the effective potential well in figure 4.  $H_a$  is measured in units of  $\sqrt{2}H_c$ , the cell radius  $a$  in units of  $\xi$ , and the force in units of  $H_c^2 \xi$ . Due to the coarse sampling, the values are only accurate to about 0.01.

Vortex–defect pinning force					
Magnetic field and defect size	Calculated from displacement–current curve	Calculated from effective potential well	Calculated from location of defect at depinning	Blatter <i>et al</i> [6]	
$H_a = 2$	$a = 0.25$	0.03	0.01	0.05	0.00357
	$a = 0.5$	0.08	0.04	0.08	0.0143
	$a = 0.75$	0.14	0.09	0.12	0.0323
	$a = 1.0$	0.17	0.10	0.15	0.0572
$H_a = 5$	$a = 0.25$	0.05	0.03	0.10	0.00357
	$a = 0.5$	0.13	0.11	0.13	0.0143
	$a = 0.75$	0.20	0.17	0.21	0.0323
	$a = 1.0$	0.26	0.24	0.27	0.0572

The values of the pinning forces obtained using all three schemes are tabulated in table 1. The resulting pinning forces have the same order of magnitude in all three cases. Furthermore, we note that the first and third approximations, both involving current-induced depinning, yield comparable pinning forces which are larger than those obtained from considering the spatial variation in the pinning potential alone. These discrepancies may be explained by the enhancement of pinning due to the increasing inner-vortex and outer-vortex interactions. This discrepancy cannot be easily removed due to the inherently nonlinear nature of the problem. However, we note that the discrepancy becomes smaller

with increasing matching field and larger defect radius, as shown in table 1. This better agreement among all three schemes may be attributed to the stronger pinning strength for larger matching field and larger defect size (figure 5), which makes the underlying assumption in the first scheme, that all vortices exterior to the cell be pinned, closer to reality.

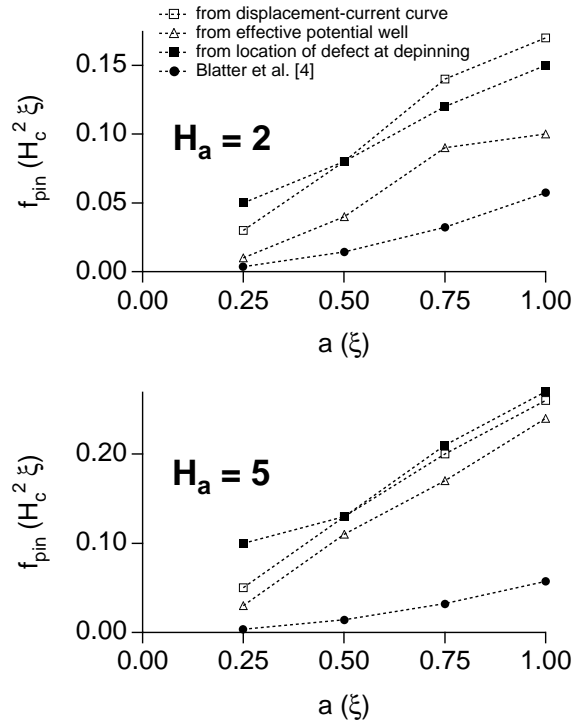


**Figure 5.** A comparison of the pinning force  $f_{pin}$  derived from various approaches described in the text as a function of the defect radius ( $a$ ) and the applied magnetic field  $H_a$ .

The above discussions consistently suggest that the magnitude of  $f_{pin}$  obtained from the spatial variation of the pinning potential (figure 4) is more accurate, particularly in the smaller- $B_\phi$  or smaller- $a$  limit. It is also interesting to note in table 1 that the pinning force per vortex increases with increasing magnetic field, provided that  $H_a \leq B_\phi$ . This seemingly surprising result is in fact due to the increasing areal density of columnar defects and the increasing vortex–vortex interaction with increasing magnetic fields, and hence the larger pinning force on vortices caused by columnar defects. We also remark that the magnetic field dependences for the first and second schemes are approximately  $f_{pin} \sim H_a$  and  $f_{pin} \sim \sqrt{H_a}$ , respectively, as shown in table 1. In the opposite limit  $H_a \gg B_\phi$  and for randomly distributed columnar defects, the vortex–pin interaction becomes equivalent to a two-dimensional collective pinning problem [6]. As stated earlier, the critical current density  $J_c^{2D}$  may be given by equation (4), provided that the  $f_{pin}$ -values obtained in our numerical calculations are inserted into equation (4). Furthermore, we note that according to equation (4)  $J_c^{2D}$  increases with increasing matching field  $B_\phi$  and decreases with increasing applied magnetic field  $H_a$ , which is qualitatively consistent with experiments [1–4].

The analysis above thus allows us to compare the relative strengths of the forces

involved, and by solving the problem for lower magnetic fields where our approximation is justified, allows us to isolate the net contribution of the vortex–defect interaction to the pinning force. These calculations for  $H_a \leq B_\phi$  can be further extended to the high-field limit  $H_a \gg B_\phi$ . It is worth noting that in addition to the qualitative agreement of our calculations with the experimental dependences of  $J_c$  on  $H_a$  and  $B_\phi$ , the magnitude of the empirical critical current densities [2–4] also agrees well with our calculated  $J_c$ -values for smaller defects with radii  $a \leq 0.5$ , measured in units of the coherence length  $\xi$ .

For further comparison, Blatter *et al* [6] estimate a depinning current based on the consideration of the single-vortex potential energy alone, and they find [6]

$$J_c = \frac{27\sqrt{2}}{64} \left(\frac{a}{2\xi}\right)^2 J_0 \simeq 0.15 \left(\frac{a}{\xi}\right)^2 J_0. \quad (9)$$

Equivalently, the depinning force per unit length obtained by such consideration yields [6]

$$\frac{f_{pin}}{H_c^2 \xi} = \frac{3\sqrt{6}}{32} \left(\frac{a}{2\xi}\right)^2 \simeq 0.06 \left(\frac{a}{\xi}\right)^2. \quad (10)$$

These estimates are in general smaller than ours by a factor of about 2 to 3 for the case of  $H_a = 2$ , and by about one order of magnitude for the case of  $H_a = 5$ . (See figure 5.) Furthermore, the result by Blatter *et al* predicts a stronger dependence of  $f_{pin}$  on the defect size than ours; i.e.,  $f_{pin} \propto a^2$  according to equation (10), in contrast to our numerical results of  $f_{pin} \sim a$ , as shown in figure 5. We note that the approach given in equations (9) and (10) by Blatter *et al* [6] does not reflect the important enhancement of  $J_c$  with larger  $B_\phi$  and with increasing vortex–vortex interactions. Furthermore, neglecting the kinetic energy contribution from the supercurrents in reference [6] also contributes to the discrepancies between their  $J_c$ -values and ours. This comparison therefore underscores the importance of considering the full solutions to the Ginzburg–Landau equations for better understanding of the vortex–pin interaction.

### 3.4. Comparison with other numerical calculations

Next, we compare the results in this work with other numerical calculations of vortex–pin interactions [13–15]. Machida and Kaburaki [13] and the research group at Argonne [14, 15] have considered the interaction of two-dimensional vortices with random defects by solving the time-dependent Ginzburg–Landau equations. However, the calculations are limited to relatively coarse grids and low values of  $\kappa$  (between 2 and 4), and therefore are not quantitatively representative of the properties of high-temperature superconductors. In addition, unlike our approach of considering the microscopic vortex–pin interaction with proper boundary conditions, the effects of defects and the resulting spatial variations of the pinning potential in references [13–15] have been assumed, rather than obtained directly from the Ginzburg–Landau equations and proper boundary conditions. While those calculations have the advantage of allowing qualitative studies of many-vortex dynamics, those results do not provide quantitative descriptions for the microscopic vortex–pin interaction of a single vortex and single defect, nor do they provide direct and accurate estimates for the critical current densities.

Recently, Reichhardt *et al* have considered the current-driven vortex dynamics in the presence of periodic pinning sites [16]. The approach considers the overdamped vortex equation of motion, and, as in most other numerical calculations [13–15], assumes given vortex–vortex and vortex–pin interactions, rather than directly solving the two-dimensional Ginzburg–Landau equations for the vortex–pin interactions and the spatial

variations of the superconducting order parameter. Nonetheless, the molecular dynamics simulations allow collective behaviour of vortices, such as novel plastic-flow phases which are uniquely associated with the periodic structure of pinning sites, to be revealed. Since the approximation involved in our calculations is generally valid for regular pinning sites, as stated previously in section 2, it would be interesting in the future to incorporate the pinning force  $f_{pin}$  and the spatial variations of the pinning potential derived from our calculations into the macroscopic studies of vortex dynamics.

### 3.5. Consideration of periodic boundary conditions

Finally, we consider solutions to the two-dimensional Ginzburg–Landau equations with periodic boundary conditions inside a rectangle. This approach is in contrast to the calculations outlined in sections 2 and 3.1 to 3.4, where boundary conditions for a circular cell have been assumed. We shall only consider the solutions in the absence of applied currents, since the presence of applied currents breaks the translational invariance required for imposing the periodic boundary conditions. Since we have demonstrated the applicability of the circular-cell solutions to a wide range of magnetic fields, the following numerical work is only to verify the energy resolution and accuracy of our calculation scheme. In other words, we show below that even in the extreme type-II limit with  $\kappa \gg 1$ , we are still able to resolve the small energy difference between the triangular and the square vortex lattices, and to obtain the small spatial variations in the order parameter and supercurrent distribution.

The solutions are obtained by using the same relaxation scheme as for the circular cells. The only difference is that the values at the boundaries are obtained from the solution on the opposite side of a rectangle with a height  $h$  along the  $\hat{y}$ -axis and a width  $w$  along the  $\hat{x}$ -axis. For simplicity, we use the gauge in which  $A_x = 0$ , and assume that the rectangle is perpendicular to the magnetic field, and the vector potential is parallel to the  $\hat{y}$ -axis. For points on the top ( $y = h$ ) or bottom ( $y = 0$ ) boundary, the values for the order parameter and for the vector potential  $A_y$  at a given  $x$ -coordinate are the same. In contrast, for points on the left-hand ( $x = 0$ ) or right-hand ( $x = w$ ) boundary, we need to adjust the phase of the order parameter and the magnitude of the vector potential. That is,

$$f(x = w) = f(x = 0)e^{iH_a w y}$$

and

$$A_y(x = w) = A_y(x = 0) + H_a w$$

where the coordinates  $x$  and  $y$  are both expressed in our dimensionless units. We note that these boundary conditions are similar to those used by Doria *et al* in their Monte Carlo solutions to the Ginzburg–Landau equations [18].

The width of the rectangles used to tile the periodic solution of the vortex system is determined by the symmetry of the vortex lattice. It must be consistent with the number of vortices per lattice cell. For a square vortex lattice, we may take, for example,  $n = 1$  or  $n = 2$  vortices per cell, and use a cell width

$$w = 2\sqrt{\pi n / (2H_a)}.$$

For a triangular vortex lattice, we need at least  $n = 2$  vortices per lattice cell, and the width becomes

$$w = (2/3^{1/4})\sqrt{\pi n / (2H_a)}$$

whereas the height of the rectangle must be kept at  $h = \sqrt{3}w$ .

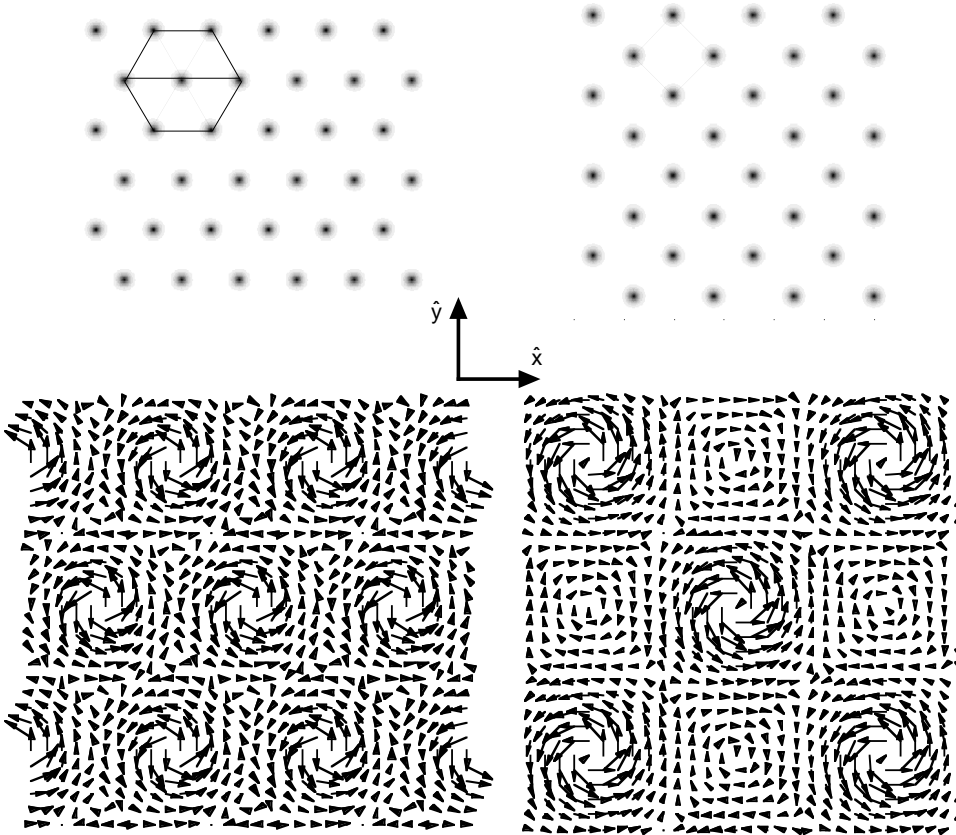


**Figure 6.** A comparison between square and triangular lattices of vortices for  $H_a = 2\sqrt{2}H_c$  and  $\kappa = 70$ . The free-energy difference per vortex (as calculated in the text) is less than one part in a thousand. Both the square and triangular lattices were obtained by tiling the solutions for  $n = 2$  vortices in square and rectangular cells, respectively. The top plot for each vortex lattice structure shows the amplitude of the order parameter, and the bottom plot the current flow (at a different scale).

Two sample (tiled) solutions using realistic parameters for high-temperature superconductors are shown in figure 6. As before, the energy can be calculated for both the square and triangular arrangements. The well known result that the energy is lower for the triangular array is obtained [19], even though the energy difference is very small due to the extreme type-II nature of the superconductor: for  $H_a = 2\sqrt{2}H_c$  and  $\kappa = 70$ , the free-energy difference per vortex between the square and the triangular lattices is *less than one part in*  $10^3$ . The scheme presented here allows us to study the energy of the vortex lattice as the angle between the lattice unit vectors changes from  $90^\circ$  (square lattice) to  $60^\circ$  (triangular lattice). Hence, we have verified the resolution and accuracy of our numerical calculations. Furthermore, the field-induced supercurrent distribution, as illustrated in figure 6, and the spatial variations of the magnetic induction (not shown), are deduced from this numerical approach.

#### 4. Conclusion

We have studied the interaction between a vortex and a columnar defect by directly solving the two-dimensional Ginzburg–Landau equations, with two different methods for deducing the pinning force: one involves imposing an external current, and the other considers the spatial variations of the pinning potential. Our numerical results using realistic material parameters for high-temperature superconductors are found to yield better descriptions for the experimental critical current densities than other theoretical work based solely on the phenomenological approach, both in terms of the magnitude and in terms of the dependences on applied magnetic field  $H_a$  and areal density of columnar defects  $n_\phi$ : we find that the critical current density  $J_c$  increases with the increasing defect size  $a$  and the matching field  $B_\phi$  for all  $H_a$ , and that  $J_c$  decreases linearly with increasing  $H_a$  for  $H_a \gg B_\phi$ . These results are direct solutions of the two-dimensional Ginzburg–Landau equations, without any assumptions as regards the spatial variations in the pinning potential.

The model presented here is quite versatile, and may be extended to studies of the interaction between multiple vortices and defects. For instance, knowing the disorder parameter  $\gamma$ , many useful physical quantities, such as the transverse vortex correlation length  $R_c \approx \varepsilon_0(\xi/4d)(d_c/\gamma)^{1/2}$ , may be obtained following the prescriptions in reference [6]. Alternatively, these quantities may be *derived* from direct numerical calculations by considering explicitly a cell with one defect and  $N$  vortices, where  $N \gg 1$ . Many other related ‘numerical experiments’ can be devised, but care must be taken in analysing the results in order to relate them to real experimental conditions.

We have also demonstrated that the numerical approach undertaken in this work provides sufficient energetic resolution to distinguish clearly the small energy difference between the configurations of triangular and square lattices, even under the extreme type-II condition. This verification indicates that our numerical schemes are quantitatively reliable. We note that all of the calculations presented in this work were done on a personal computer, and thus they can be easily extended to large systems, higher dimensionality, more complex boundary conditions, etc, with a more powerful computing system. Finally, it will be interesting to generalize our numerical approach to incorporate both the s-wave and d-wave components of the order parameter in the Ginzburg–Landau equations [20], so that the vortex–pin interactions in d-wave superconductors may be compared with those obtained in s-wave superconductors.

#### Acknowledgments

SM would like to acknowledge support from Caltech’s Ph11 and the Summer Undergraduate Research (SURF) programs that made his participation possible. SM also thanks Brian D’Urso for helpful discussions on the numerical algorithms. The work was supported in part by the National Science Foundation (Grants DMR94-01315 and DMR93-18931), the Office of Naval Research (Grant N00014-91-J-1556), and the David and Lucile Packard Foundation.

#### References

- [1] Konczykowski M, Rullieralbenque F, Yacoby E R, Shaulov A, Yeshurun Y and Lejay P 1991 *Phys. Rev. B* **44** 7167
- [2] Civale L, Marwick A D, Worthington T K, Kirk M A, Thompson J R, Krusin-Elbaum L, Sun Y, Clem J R and Holtzberg F 1991 *Phys. Rev. Lett.* **67** 648

- [3] Krusin-Elbaum L, Civale L, Blatter G, Marwick A D, Holtzberg F and Feild C 1994 *Phys. Rev. Lett.* **72** 1914
- [4] Baert M, Metlushko V V, Jonckheere R, Moshchalkov V V and Bruynseraede Y 1995 *Phys. Rev. Lett.* **74** 3269
- [5] Nelson N R and Vinokur V M 1992 *Phys. Rev. Lett.* **68** 2398  
Nelson N R and Vinokur V M 1993 *Phys. Rev. B* **48** 13060
- [6] Blatter G, Feigel'man M V, Geshkenbein V B, Larkin A I and Vinokur V M 1994 *Rev. Mod. Phys.* **66** 1327
- [7] Jiang W, Yeh N-C, Reed D S, Beam D A, Kriplani U, Konczykowski M and Holtzberg F 1994 *Phys. Rev. Lett.* **72** 550  
Reed D S, Yeh N-C, Konczykowski M, Samoilov A V and Holtzberg F 1995 *Phys. Rev. B* **51** 16448  
Reed D S, Yeh N-C, Jiang W, Kriplani U, Konczykowski M and Holtzberg F 1996 *Int. J. Mod. Phys. B* **10** 2723
- [8] Samoilov A V, Feigel'man M V, Konczykowski M and Holtzberg F 1996 *Phys. Rev. Lett.* **76** 2798 (erratum 1996 **77** 981)  
Civale L and Krusin-Elbaum L 1997 *Phys. Rev. Lett.* **78** 1829 (comment)  
Konczykowski M and Samoilov A V 1997 *Phys. Rev. Lett.* **78** 1830 (reply)
- [9] Thuneberg E V 1984 *J. Low Temp. Phys.* **57** 415  
Thuneberg E V, Kurkijarvi J and Rainer D 1984 *Phys. Rev. B* **29** 3913
- [10] Friesen M and Muzikar P 1997 *Phys. Rev. B* **55** 509
- [11] Maurer S M, Yeh N-C and Tombrello T A 1996 *Phys. Rev. B* **54** 15372
- [12] The computations were performed on a 60 MHz PowerPC 601 desktop computer with 16 (and later 40) Mbyte of RAM. In some case, solutions for a single vortex and a single defect could take up to half an hour on large (320 by 320) grids.
- [13] Machida M and Kaburaki H 1995 *Phys. Rev. Lett.* **75** 3178
- [14] Aranson I, Shapiro B Ya and Vinokur V M 1996 *Phys. Rev. Lett.* **76** 1170
- [15] Braun D W, Crabtree G W, Kaper H G, Koshelev A E, Leaf G K, Levine D M and Vinokur V M 1996 *Phys. Rev. Lett.* **76** 831
- [16] Reichhardt C, Olson C J and Nori F 1997 *Phys. Rev. Lett.* **78** 2648
- [17] de Gennes P G 1966 *Superconductivity of Metals and Alloys* (New York: Benjamin)
- [18] Doria M M, Gubernatis J E and Rainer D 1990 *Phys. Rev. B* **41** 6335
- [19] Abrikosov A A 1957 *Zh. Eksp. Teor. Fiz.* **32** 1442 (Engl. Transl. 1957 *Sov. Phys.-JETP* **5** 1174)  
Kleiner W H, Roth L M and Autler S H 1964 *Phys. Rev.* **133** A1226
- [20] Berlinsky A J, Fetter A L, Franz M, Kallin C and Soinenen P I 1995 *Phys. Rev. Lett.* **75** 2200  
Franz M, Kallin C, Soinenen P I, Berlinsky A J and Fetter A L 1996 *Phys. Rev. B* **53** 5795